Powder Technology 382 (2021) 478–490

Contents lists available at ScienceDirect

Powder Technology

journal homepage: www.elsevier.com/locate/powtec

Compaction behavior and densification mechanisms of Cu—W composite powders

Kefeng Peng [a], Hao Pan [b], Zhijun Zheng [a,*], Jilin Yu [a]

[a] CAS Key Laboratory of Mechanical Behavior and Design of Materials, Department of Modern Mechanics, University of Science and Technology of China, Hefei, Anhui 230027, China
[b] Institute of Applied Physics and Computational Mathematics, Beijing 100088, China

ARTICLE INFO

Article history:
Received 10 August 2020
Received in revised form 5 January 2021
Accepted 7 January 2021
Available online 11 January 2021

Keywords:
Multi-particle finite element method
Cu-W composite powders
Compaction
Meso-structure
Densification mechanisms
Quantitative characterization

ABSTRACT

The deformation mechanism related to the initial relative density and uniformity of Cu—W composite powders under quasi-static compression was investigated by multi-particle finite element method. The results show that under the same pressure, the relative density of powder increases with the increase of initial relative density or the uniformity of composite powders. The densification processes can be divided into three stages, namely particle rearrangement, Cu particle deformation and W particle deformation. Pores are mainly filled by the rearrangement of particles and the deformation of Cu particles. The rearrangement and deformation of particles are quantitatively characterized by introducing the mean rotation degree and the mean equivalent strain of powders. It is found that smaller voids formed in the initial denser powder are easily filled by the deformation of adjacent particles during compaction. Strong force chains formed by the contact of W particles severely hinder the compression, resulting in large porosity.

1. Introduction

Composite granular materials have drawn great attention in many industrial areas, such as aerospace, electronics, medical devices and industrial metallurgy, due to their improved properties with the advantages of high specific strength, multi-scale, fluidity, permeability and heat insulation, as well as low price of raw materials [1–3]. Among a variety of composite granular materials, Cu—W binary composite materials have good characteristics, such as high hardness, high temperature performance, strong wear resistance and excellent corrosion resistance [4–7], and thus the fabrication of Cu—W intermetallic granular materials gets increasingly important. Powder metallurgy is a competitive and promising manufacturing method for tungsten metals and alloys, which can reduce segregation and produce products with special structures and properties. In the process of powder metallurgy, the compaction and sintering stages play dominant roles in preparing superior products. Some work focused on the sintering stage has been studied to explore the effects of sintering temperature and heating rate in the literature [8,9], and some research interest about powder metallurgy at the compaction stage has also been raised [10]. In fact, in order to form high performance products, one should pay much attention to the adjustable parameters in the compaction stage, since compaction with small and uniform pore size, high relative density and uniform stress is the prerequisite of the preparation of superior composites. Besides, producing high-quality products by controlling the meso-structures of powder rather than by optimizing the design of compaction die [11,12] may be an efficient way, and deep studies on the mesoscopic deformation mechanisms of composite powders during compaction are required.

Experimental and numerical methods have been employed to study the compaction of powder. Extensive experiments were conducted and focused on the relationship between mean relative density and compression pressure [13–16]. However, experiments may be limited in the quantitative description of relative density distribution, stress distribution and powder flow behavior, since the non-linear features, including material nonlinearity, geometric nonlinearity and contact nonlinearity, greatly increase the difficulties in physical experimental analysis. To overcome this shortcoming, a discrete element method (DEM), which stems from the studies of granular flow and soil mechanics [17], was developed. The DEM has been widely used to generate random packing structures with spherical or non-spherical particles and successfully applied to compression [18], shear [19] and vibration [20] simulations. The DEM could be used for predicting the elasticity and strength of green compacts [21], but it might be limited to small deformation, resulting in a relative density of less than 0.85 for powder compaction [22]. To alleviate the difficulties associated with DEM, a multi-particle finite element method (MPFEM) with full finite element discretization of the particles was developed in recent years. A direct advantage of this method is to offer great flexibility in particle shape and

* Corresponding author.
E-mail address: zjzheng@ustc.edu.cn (Z. Zheng).

https://doi.org/10.1016/j.powtec.2021.01.013
0032-5910/

contact deformation. It can simulate the compaction process to a higher relative density without any simplification. Gethin et al. [23] applied this method to fix a compaction problem, in which a dozen of particles were arranged in a periodic manner. Recently, the MPFEM was substantially developed by Zavaliangos [24,25] and Frenning [26,27]. This method is able to deal with many issues for powder compaction, such as particle deformation and yield surface [25,28], thermal conductivity [29], effects of friction [30], size ratio [31] and particle packing [32,33]. The MPFEM has also been utilized in the studies on the forming of different metals, alloys and composites [34–36], but most of them are restricted to be two-dimensional, which may bring some differences with the real three-dimensional powder. In particular, based on the MPFEM, multi-scale analysis of the compaction behavior of composite powders can be carried out. This may promote the understanding of the densification mechanism and optimize the adjustable parameters in the production process and thus improve the product quality.

Some work has been done to study the effects of material/structural parameters on the powder densification process, and the effects of initial packing density and particle distribution may be vital in the densification process. Particle distribution determines the uniformity of composite powders. Normally, uniform powders produce high quality products, but the micro-deformation mechanism is unclear and it is necessary to characterize the property of powder compaction involving powder uniformity. In addition, as a primary parameter, initial packing density has an important influence on the packing structure and corresponding properties [37]. The results reported in Refs. [38–40] showed that single powders with different initial packing densities exhibit different densification capacity, i.e. at a given pressure, the relative density of the initially dense powder is higher than that of the initially loose powder. While for composite powders, the effects of the initial packing density on the powder densification process are still unclear. More importantly, densification dynamics and mechanisms of composite powders with different initial packing densities and particle distribution need to be systematically and thoroughly studied, and the understanding of the correlation between macroscopic mechanical responses and microscopic particle mechanics of composite powders compaction is desired.

In this study, a 3D multi-particle finite element model subjected to single action die compaction with a low constant velocity was employed in the numerical simulations to understand the quasi-static compression behaviors of Cu—W composite powders. We focus on the effect of the initial relative density and the distribution of W and Cu particles on the compression behavior through the model with the same Cu content, particle shape and particle numbers. The mechanical responses, e.g. the relationship between pressure and relative density, and some mesoscopic properties, including relative density distribution and stress distribution, were illustrated and the corresponding densification mechanisms were explored.

2. Numerical simulation

Random packing structures were generated to simulate the assemblies of Cu—W composite powders in a cuboid container with a volume of $\Omega_c = 10 \times 10 \times 40\ \mathrm{mm}^3$. The packing structures can be characterized by the initial relative density ρ_0 and the Cu content α. Here, α is defined as the volume fraction of Cu particles in Cu—W composite powders and ρ_0 is defined as Ω_0/Ω_s with Ω_0 being the volume of the composite powders and Ω_s the volume of a cube that exactly holds all the particles, here $\Omega_s = 10 \times 10 \times H\ \mathrm{mm}^3$ and H is the height of the composite powders. For the sake of simplicity, we consider that all particles have an equal radius, which is set as 1 mm in this study. Discrete element method was commonly used to obtain a random packing structure of powder, which can more realistically reflect the actual filling process [5,28,34]. Thus, this method was applied to fill particles into the container [41]. The generation of mesoscale geometric model consists of three steps:

i). Points are scattered randomly and their coordinates are taken as the initial positions of particle nuclei according to the predetermined particle numbers. In the finite element simulation, due to the limitation of CPU time, the number of particles cannot be too much. The requirement of the number of particles was to approach a representative volume element of the powder. By validating with experiments, the number of particles in the literatures of MPFEM simulation is mostly between 32 and 132 [5,28,34]. In this study, 190 particles were used in a specimen.

ii). The particle positions are updated to ensure that the distance between any two points is not less than the particle diameter and no particle is outside the boundary by using the delay algorithms of contact mechanics with the consideration of a virtual gravity and a 3D vibration boundary condition. The vibration boundary condition acting on the walls of the container is given by $u = d\sin(2\pi ft)$, where u is the displacement, d is the amplitude, f is the vibration frequency and t is the vibration time. More details about the vibration boundary condition can be found in Ref. [42]. In this study, the values of d and f are 0.1 mm and 20 Hz, respectively. It is worthy to note that in the DEM simulation, the particles are identical to avoid segregation. The implement of DEM simulation only aims to provide the geometrical location of particles.

iii). Once the particle location is fixed, the Cu particles are assigned randomly on the basis of the proportion of Cu particles and the rest is taken as the W particles. It is noted that the present numerical generation method of composite powders can be applied to control the initial packing density by 3D vibration, while it cannot be used to control the uniformity of composite powders due to the random choice of Cu particles.

A local inhomogeneity index for a meso-structure identified by the center particle c with its surrounding particles is introduced to measure the inhomogeneity of a local packing structure at meso-scale, given by

$$\gamma_c = \frac{n_c^{\mathrm{Cu}}}{n_c} - \alpha \tag{1}$$

where n_c is the number of particles in the c-th meso-structure (particles adjacent to c and c itself), n_c^{Cu} is the number of Cu particles in the c-th meso-structure, and α is the volume fraction of Cu particles in the Cu—W composite sample. The inhomogeneity of the whole composite powders could be characterized by the average local inhomogeneity index of all meso-structures, expressed as

$$\gamma = \sqrt{\frac{1}{N}\sum_{c=1}^{N}{\gamma_c}^2} \tag{2}$$

The smaller the value of γ is, the more uniform the composite powder is. As a random packing process applied, the inhomogeneity index of each sample may be different. Some samples with a Cu content of 50% and an initial relative density of 0.526, but having different inhomogeneity indexes, are presented in Fig. 1. It is worth noting that the particle positions of these samples are identical, and the only difference is the Cu and W particle distribution. Maintaining the same initial stacking structure can avoid the dispersion of the structure and the effect of the uniformity of composite powders can be considered alone. In addition, it is worthy to mention that the Cu—W composite powders with Cu content of 50% are widely applied in the fabrication of Cu—W functionally graded materials [43–45] and are promising candidates for electrical contacts and shaped charge liner materials in military applications [6,7].

The initial packing density can be controlled by the vibration time and the inter-particle friction in the DEM simulation. The longer the vibration time or the smaller the friction coefficient is, the higher the initial packing density is [42]. Some samples with a Cu content of 50% and

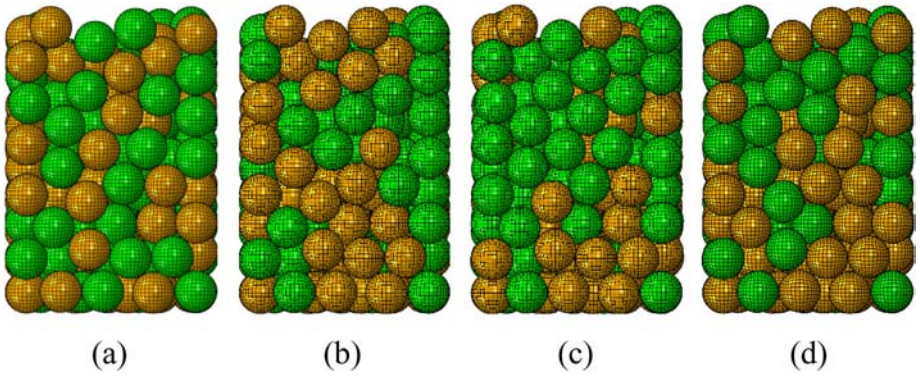

Fig. 1. Initial configurations of Cu–W composite powders with the same Cu content of $\alpha = 50\%$ and initial relative density of $\rho_0 = 0.526$, but different inhomogeneity indexes: (a) $\gamma = 0.036$, (b) $\gamma = 0.044$, (c) $\gamma = 0.054$ and (d) $\gamma = 0.063$.

an inhomogeneity index of about 0.036, but having different initial relative densities, are presented in Fig. 2.

The quasi-static compression process of Cu—W composite powders was simulated by using finite element code ABAQUS/Explicit. Each particle was meshed individually and then imported into the finite element software. According to the grid convergence analysis, each particle is divided into 2048 hexahedral elements (C3D8R) with 2273 nodes, as illustrated in Fig. 3(a). The bulk materials of Cu and W are assumed to be elastic-plastic with Young's modulus E, Poisson's ratio ν and density ρ_s listed in Table 1. The yield stress of the matrix materials was assumed to follow the Johnson–Cook model [46] as

$$\sigma_Y = (A + B\varepsilon^n)\left[1 + C\ln\left(\dot{\varepsilon}/\dot{\varepsilon}_0\right)\right]\left\{1 - \left[(T - T_{melt})/(T_{melt} - T_{room})\right]^m\right\} \quad (3)$$

where A, B, C, n and m are material constants. A is the initial yield stress, B the hardening constant, C the strain rate sensitivity index, $\dot{\varepsilon}$ the strain rate (the reference strain rate $\dot{\varepsilon}_0 = 1\ s^{-1}$), n the hardening index, m the temperature softening coefficient, T_{melt} the melting point and T_{room} the room temperature. These material parameters for the Cu and W used in this study are obtained from Ref. [47] and are listed in Table 1. Besides, the specific heat and thermal expansion coefficients of Cu and W are obtained from Refs. [47, 48]. The specific heat of Cu is 386 J/kg/K and that of W is 134 J/kg/K. The thermal expansion coefficient is a temperature-related variable and the data of Cu and W are given in Figs. 12 and 40 of the Ref. [48].

The specimens are confined in a rigid cuboid container for the simulation of the actual closed-die compression. The walls of the fixture are fixed except the one at the loading end. Compression is carried out through the rigid plate at the loading end, which moves to the support end at a constant velocity of $V = 1$ m/s, as shown in Fig. 3(b). The

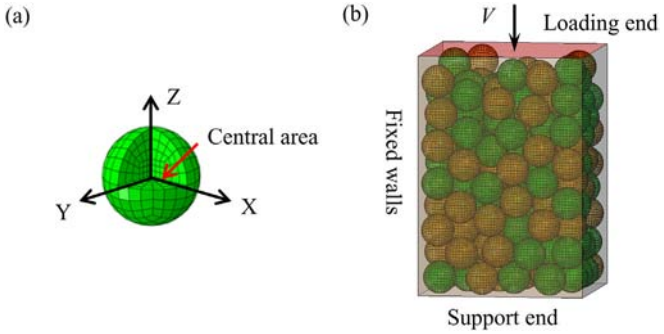

Fig. 3. (a) The initial mesh of a particle; (b) a finite element model of Cu–W composite powders under constant-velocity compression.

explicit analysis of stiff particles is time-consuming and an excessively small time step may occur. Thus, in the calculation, the semi-automatic mass scaling with a target time increment of 2×10^{-6} ms is used to increase the critical time step, and the loading time of a sample is about 7.5 ms. The coefficient of friction between particles is difficult to determine and the particle-wall friction is complex because of its dependence on the lubrication condition, contact pressure, particle flow behavior, etc. Thus, for simplicity, the friction coefficient between the particles is set to be 0.2 and there is no friction between particles and the rigid walls in this study, as used in Refs. [5, 35–37].

The numerical models were validated by comparing the present results and the experimental results in the literature [49], where the composite powders with an initial relative density of 0.61 and Cu contents of

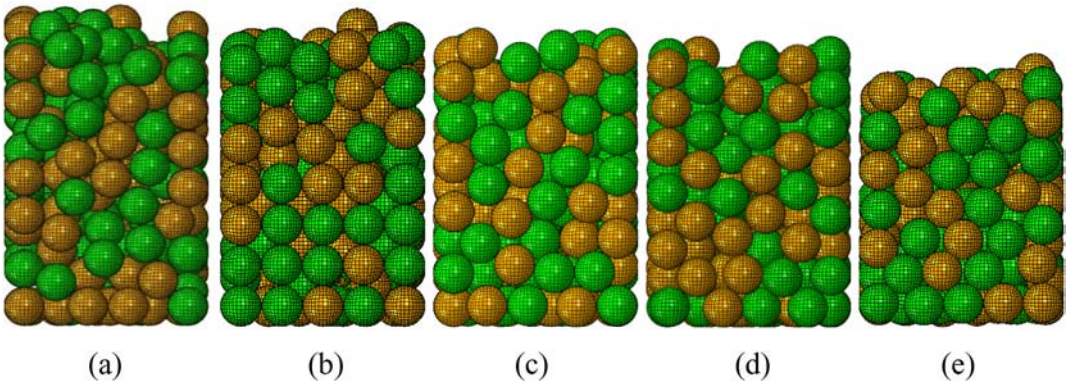

Fig. 2. Initial configurations of Cu–W composite powders with the same Cu content of $\alpha = 50\%$ and inhomogeneity index of $\gamma = 0.036$, but different initial relative densities: (a) $\rho_0 = 0.476$, (b) $\rho_0 = 0.510$, (c) $\rho_0 = 0.526$, (d) $\rho_0 = 0.537$ and (e) $\rho_0 = 0.558$.

Table 1
Material parameters of Cu and W [47].

Material	ρ_s (kg/m^3)	E (GPa)	ν	A (MPa)	B (MPa)	C	n	m	T_{room} (K)	T_{melt} (K)
Cu	8930	124	0.34	90.0	292	0.025	0.31	1.09	300	1360
W	17,800	133	0.22	1510	177	0.016	0.12	1.0	300	3660

20%, 40% and 60% were compacted under pressures of 150–650 MPa. The corresponding compaction pressure p vs. relative density ρ curves are plotted in Fig. 4. The relative density ρ is calculated by Ω_0/Ω_d, where Ω_d is the volume of the die during compaction. For accuracy of comparison, the parameters of bulk materials W and Cu used for these simulation samples are the same as those in Ref. [49]. The inhomogeneity of composite powders is not stated in Ref. [49] and thus the inhomogeneity indexes of the samples simulated here are considered to be random. The results of the p–ρ curves obtained from MPFEM simulation and experimental tests show similar trends, although those from MPFEM simulation are a little lower than those of the experimental tests. This may be caused by the difference in meso-parameters, such as particle shape and powders uniformity in simulation and experiment. Nevertheless, it is found that the MPFEM is an efficient method to simulate the compaction of Cu—W powders. Besides, from Fig. 4, it could also be found that in MPFEM simulation, the pressure at the loading end is almost equal to that at the support end, indicating the compression velocity of 1 m/s is low enough to simulate a quasi-static compaction process.

3. Results and discussion

3.1. Mechanical responses of composite powders with different uniformities

3.1.1. Features of deformation, stress and temperature distribution

Samples with inhomogeneity indexes of 0.036, 0.044, 0.054 and 0.063, as shown in Fig. 1, under compression at a velocity of 1 m/s were simulated. The deformation patterns and von Mises stress distribution of these samples under pressure $p = 500$ MPa are shown in Fig. 5. The results indicate that the uniformity of composite powders indeed has a significant influence on the powder compaction. Firstly, under a pressure of 500 MPa, the mean relative densities of these samples are 0.856, 0.850, 0.844 and 0.842, respectively, so the relative density decreases with the increase of the inhomogeneity index. Secondly, it is noticed that the local von Mises stress distribution is inhomogeneous in these samples, and the divergence in the von Mises stress is much obvious in the non-uniform samples. Thirdly, the concentrated accumulation of W particles in the samples with high inhomogeneity index forms strong force chains, which are represented by the white lines in Fig. 5. The strong force chains greatly increase the compression resistance, hinder the filling of pores, and further lead to the uneven distribution of pores, as can be seen in Fig. 5.

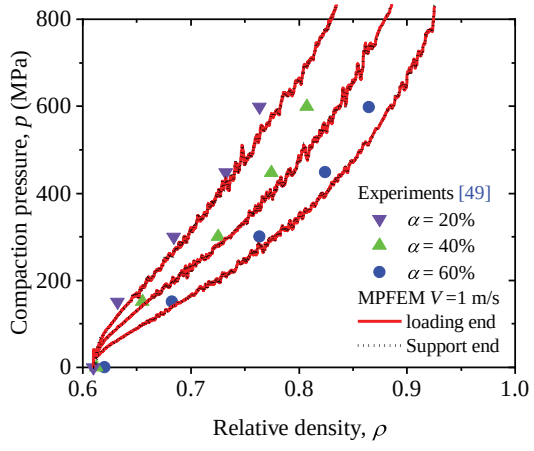

Fig. 4. Comparison of the compaction pressure and relative density curves between MPFEM simulation and experiments.

It is recognized that temperature is the dominant factor in the sintering stage [5]. However, the temperature evolution and distribution in the compaction stage are rarely studied, which may affect the subsequent powder metallurgy process since the high temperature, which is necessary for local metallurgical bonding at the interfaces of powder, may be generated under compaction. Therefore, the temperature evolution and distribution in the compaction stage are analyzed here. The temperature distribution was obtained from the finite element simulation, which is calculated according to the specific heat and the thermal expansion coefficients of Cu and W particles. The temperature evolutions of Cu—W composite powders with an initial relative density of 0.526, a Cu content of 50% and an inhomogeneity index of 0.036 under different pressures of 200, 300, 500 and 800 MPa were plotted in Figs. 6(a)–(d). The results show that the temperature distributions in the composite powders are uneven. High temperature mainly concentrates on the area of contacted W particles and the boundary near the rigid walls. The temperature in the composite powders increases with the increase of the compaction pressure. Thus, local bonding appears under high compaction pressure when the temperature exceeds the melt temperature of Cu or W particles. The effects of uniformity of composite powders on the temperature distribution are further explored. The temperature distributions of Cu—W composite powders with an initial relative density of 0.526 and a Cu content of 50% but different inhomogeneity indexes of 0.036, 0.044, 0.054 and 0.063 under a pressure of 500 MPa were illustrated in Figs. 6(e)–(h). It is found that the temperature in the outer area of particles is greater than that in the interior of the particles. The uniformity of composite powders seems to have no obvious effects on the temperature distribution. The analysis of temperature distribution in the compaction stage can be used as a basis for the subsequent sintering process, and this analysis method can also be applied to guide hot pressing.

The compaction pressure p vs. relative density ρ curves of Cu—W composite powders with different inhomogeneity indexes are shown in Fig. 7. It is noticed that with the increase of uniformity, the compressibility of composite powders is significantly improved under relatively high pressure ($p > 300$ MPa), indicating that the Cu—W distribution of composite powders plays an important role in the densification stage. However, the discrepancy of the p–ρ relationship at the initial compression stage is hardly observed from Fig. 7. The reason may be that the deformation mechanism is different under different pressures, which will be analyzed in the next section.

The Heckel empirical equation [50] has been commonly suggested to fit the results for powder compression, which is written as

$$-\ln(1-\rho) = \lambda p + \beta \tag{4}$$

where β is related to low pressure densification by inter-particle movement and λ is a measure of compressibility by plastic deformation of particles. The fitting results of the cases with inhomogeneity indexes of 0.032 and 0.063 are shown in Fig. 8(a) and the values of λ and β corresponding to different inhomogeneity indexes are plotted in Fig. 8(b). As can be seen, the value of λ decreases with the increase of the inhomogeneity index. On the other hand, the value of β keeps stable, and thus the inter-particle movement is almost independent of the uniformity of powders.

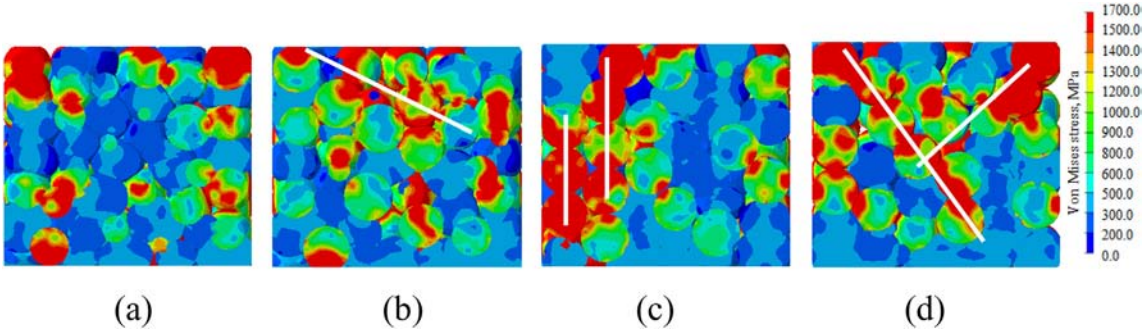

Fig. 5. Deformation patterns and von Mises stress distribution of Cu—W composite powders with an initial relative density of 0.526 and a Cu content of 50% but different inhomogeneity indexes of: (a) 0.036, (b) 0.044, (c) 0.054 and (d) 0.063 under a pressure of 500 MPa. The white lines represent the strong force chains.

3.1.2. Quantitative characterization of the particle rearrangement and deformation

The deformation mechanisms of metal powder under compaction usually include particle rearrangement and plastic flow. These mechanisms may occur simultaneously, but any of them may take the primary role under different pressures. However, it is difficult to identify various deformation mechanisms from the p–ρ relationship due to the coupling effects of particle rearrangement and deformation. Therefore, in order to better understand the densification mechanism, it is necessary to quantitatively and separately characterize particle rearrangement and deformation. Since the rotation of particles is much flexible at the rearrangement stage, and the particle rotation is insensitive to the deformation of particles, thus the rotation of particles is introduced here to represent the rearrangement of particles. It may be difficult to precisely describe the particle rotation since the particles are deformable during compaction. However, we observed that the central area of a particle is almost free of deformation even under high pressure and thus could be taken as a reference of particle orientation (see Fig. 3(a)). Then the quaternions, which can describe 3D rotations of a rigid body, are employed to represent the rotation degree of a particle and defined as [51].

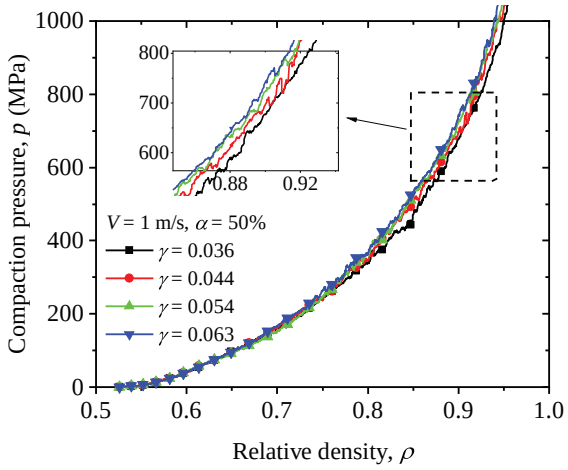

Fig. 7. Evolution of the relative density of Cu—W composite powders with different inhomogeneity indexes with compaction pressure.

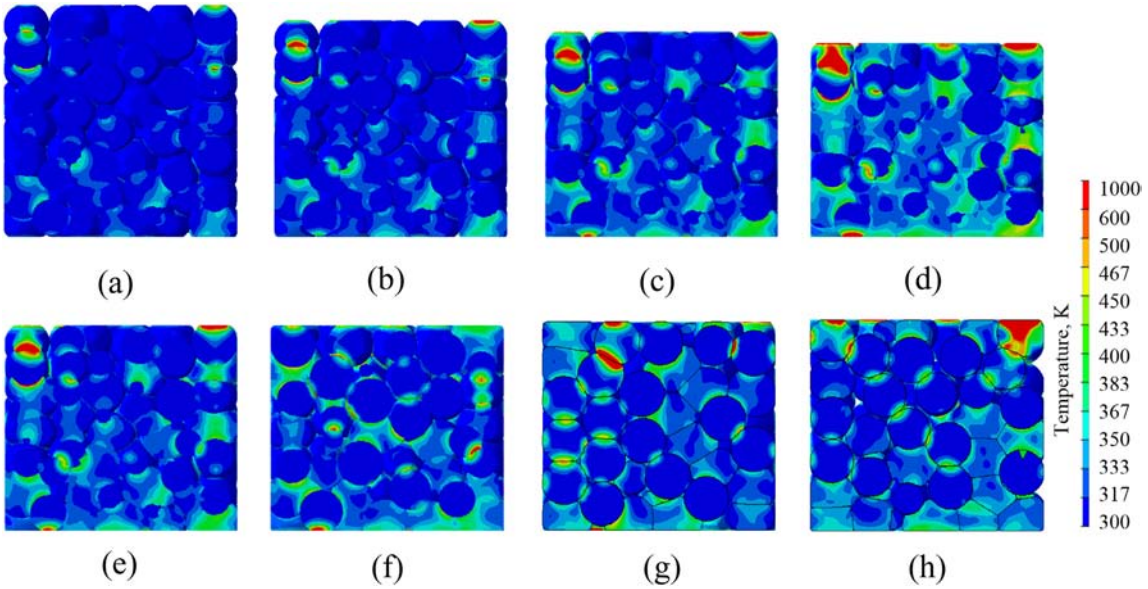

Fig. 6. Temperature evolution of Cu—W composite powders with an initial relative density of 0.526, a Cu content of 50% and an inhomogeneity index of 0.036 under different pressures of (a) 200 MPa, (b) 300 MPa, (c) 500 MPa and (d) 800 MPa. Temperature distribution of Cu—W composite powders with an initial relative density of 0.526 and a Cu content of 50% but different inhomogeneity indexes of (e) 0.036, (f) 0.044, (g) 0.054 and (h) 0.063 under a pressure of 500 MPa.

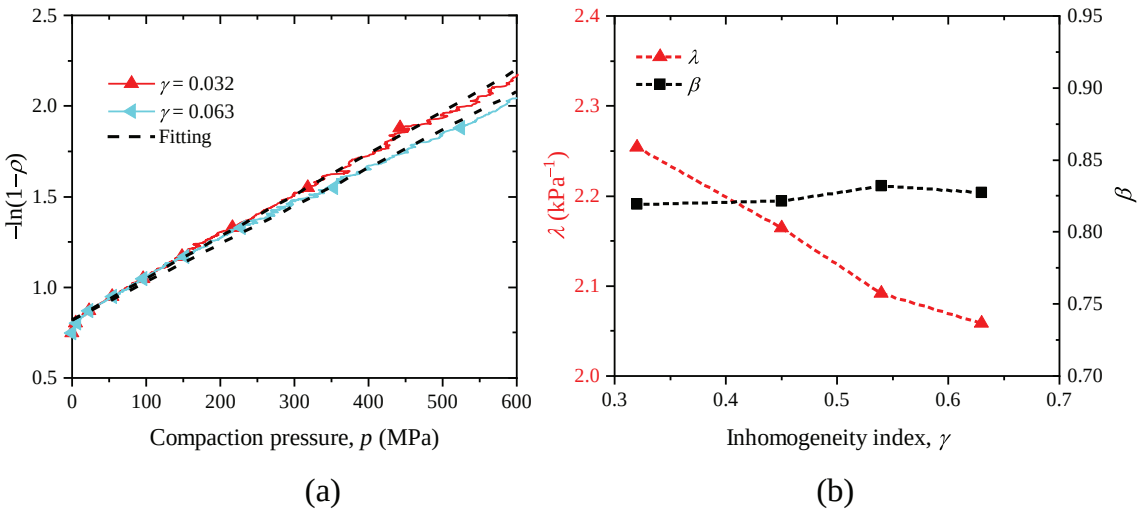

Fig. 8. (a) Fitting the MPFEM data with the Heckel equation and (b) the values of parameters λ and β in the Heckel equation with different inhomogeneity indexes.

$$\theta = 2\arccos\left(\prod_{k=1}^{3}\cos\frac{\theta_k}{2} + \prod_{k=1}^{3}\sin\frac{\theta_k}{2}\right) \tag{5}$$

where θ_k represents the rotation degree in direction j and $k = 1, 2, 3$ are the three main axes (X, Y, Z) of a particle. As for particle deformation, the average equivalent strain ε_{eq} of powders is used to represent the deformation of particles, defined as [5].

$$\varepsilon_{eq} = \frac{1}{N}\sum_{i=1}^{N}\left(\varepsilon_p^i + \varepsilon_e^i\right) \tag{6}$$

where N is the number of particles in the composite powders considered, ε_p^i and ε_e^i are the equivalent plastic strain and equivalent elastic strain of the i-th particle, which are calculated by the mean plastic strain and mean elastic strain of the elements that constructing the particle, respectively, given by

$$\begin{cases} \varepsilon_p^i = \dfrac{1}{\Omega}\sum_{j=1}^{N_E}\varepsilon_{pE}^j\Omega_E^j \\ \varepsilon_e^i = \dfrac{1}{\Omega}\sum_{j=1}^{N_E}\varepsilon_{eE}^j\Omega_E^j \end{cases} \tag{7}$$

where N_E is the element number in a particle, Ω_E^j is the volume of the j-th element in the particle, Ω is the volume of the particle, and ε_{pE}^j and ε_{eE}^j are the plastic and elastic strains of the j-th element in the particle, respectively. As can be seen from Fig. 9, initially (Stage 1), with the increase of the relative density, the mean rotation degrees of W and Cu particles increase quickly and the mean equivalent strains of W and Cu powders are nearly zero. Thus, at this stage, the densification process is dominated by particles rearrangement. After reaching the locked state (Stage 2), the rearrangement of the particles is limited, resulting in a slow increase in the rotation degrees of the particles. In this stage, the Cu particles are deformed to fill their adjacent pores, while the W particles are hardly deformed. At the final stage (Stage 3), the deformation of W particles increases, thereby further squeezing Cu particles and causing more rotation of Cu particles. Thus, the difference between the rotation degree of W particles and Cu particles increases, as shown in Fig. 9 (b). It can be seen that the three stages can be observed for each sample, which are in agreement with the results obtained in the literature [31,32,35,36].

The effects of the uniformity of composite powders on the particle rearrangement and deformation are explored. As can be seen from Fig. 10 (a), the mean equivalent strains of Cu—W composite powders with dif-

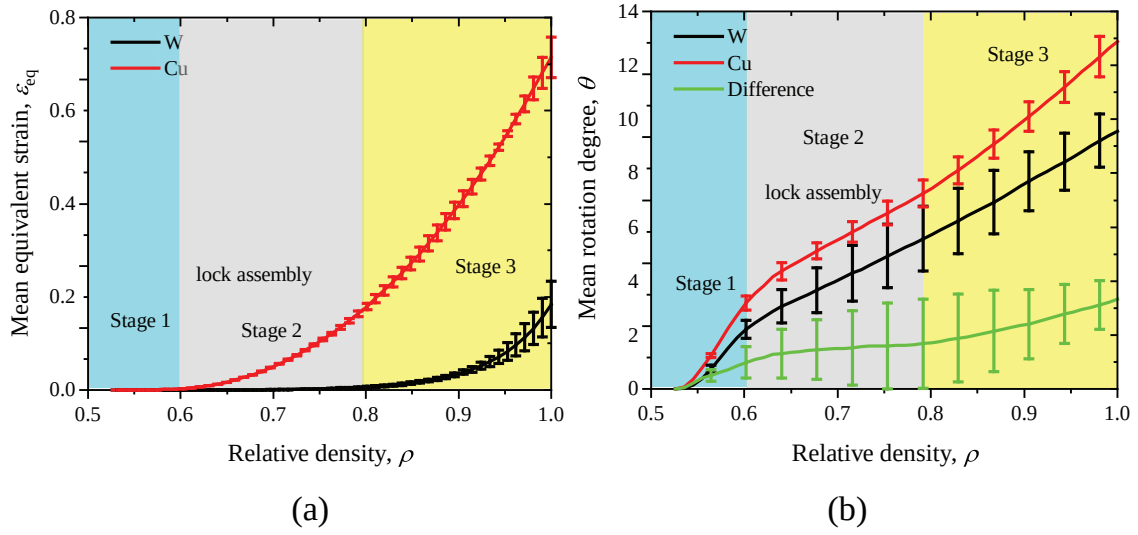

Fig. 9. The mean equivalent strains (a) and the mean rotation degrees (b) of Cu and W particles.

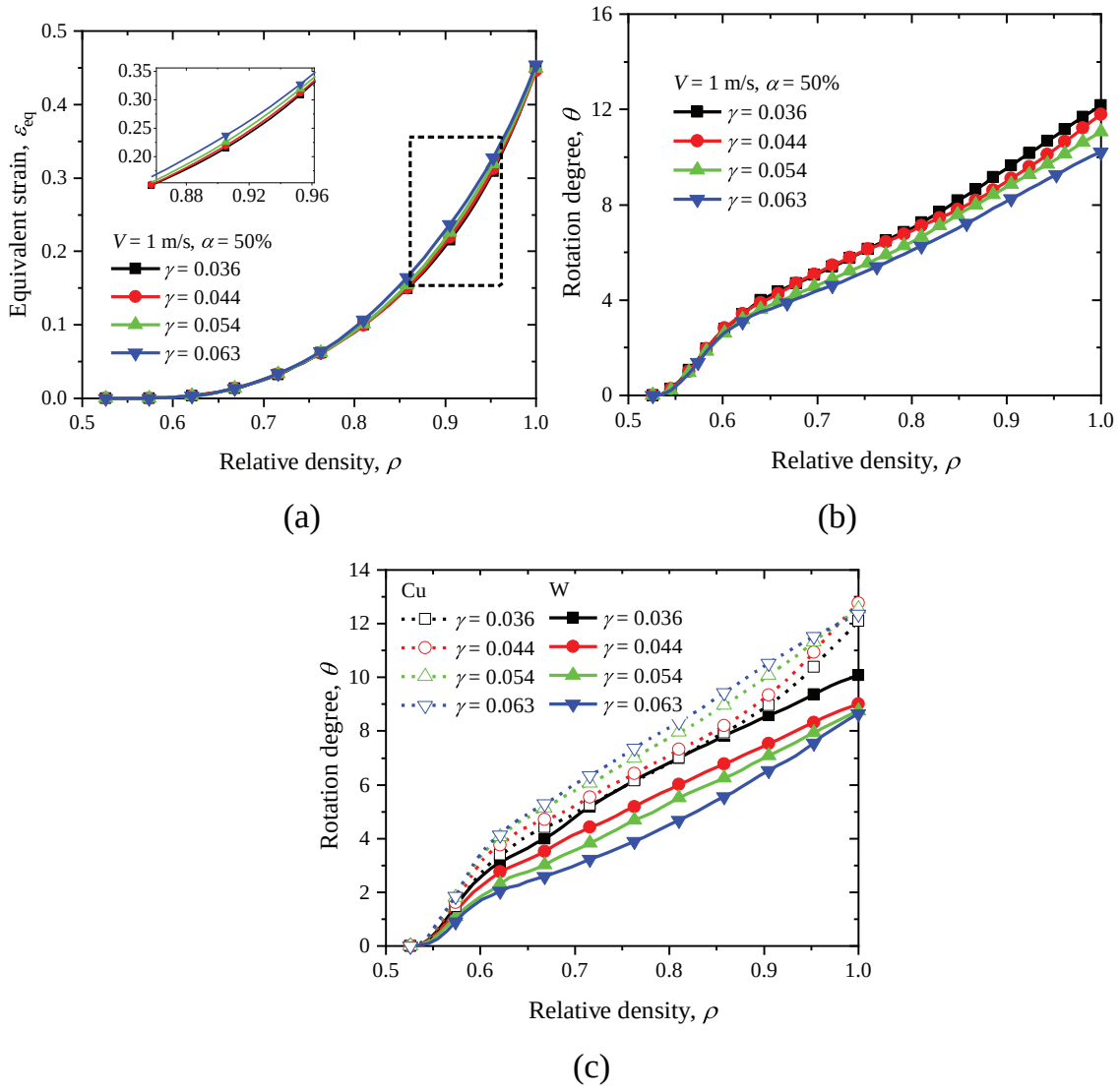

Fig. 10. The mean equivalent strains (a) and the mean rotation degrees (b) of Cu—W composite powders with different inhomogeneity indexes. (c) Rotation degrees of Cu and W particles.

ferent inhomogeneity indexes are almost identical at the initial compression stage and the difference occurs at the subsequent compression stages, in which the mean equivalent strain of the composite powders with high inhomogeneity index is larger than that of the composite powders with low inhomogeneity index. Similarly, for the Cu—W composite powders with different inhomogeneity indexes, the mean rotation degrees are almost equal and rise quickly at the initial compression stage. At the subsequent compression stages, the mean rotation degree increases slowly. The more uniform the composite powders are, the larger the mean rotation degrees are, as shown in Fig. 10(b). The rotation degrees of Cu and W particles are plotted in Fig. 10(c). It is found that with the increase of the inhomogeneity index, the rotation degree of W particles decreases, while that of Cu particles increases. Obviously, the change of rotation degree of W particles is greater than that of Cu particles, which can be explained by that during compaction, W particles are hardly deformed and thus the contacted W particles can form relatively stable packing structures to resist motion. Once the stable packing structures are disrupted, the W particles in the structures will move easily. While for Cu particles, they are easily deformed to restrict their movement and thus the change of their rotation degrees is relatively small. In addition, the more uniform the composite powders are, the less the difference in rotation degrees between Cu and W particles is. The reason may be that under compression, the Cu particles deformed concavely and then locked their adjacent W particles. In general, particle rearrangement not only occurs at the initial compression stage, but also takes an important role at the subsequent compression stages. Besides, the results show that at the initial compression stage, the particle rearrangement is not sensitive to the uniformity of composite powders, while the particle deformation is closely related to the particle distribution.

Particle translation can also be used to characterize the particle rearrangement. A normalized displacement is introduced to represent the translational motion of the i-th particle, defined as

$$d_i = \frac{1}{H}\sqrt{\left(X^i - x^i\right)^2 + \left(Y^i - y^i\right)^2 + \left(Z^i - Z^i\varepsilon_N - z^i\right)^2} \tag{8}$$

where (x^i, y^i, z^i) and (X^i, Y^i, Z^i) are the current and initial locations of the i-th particle, respectively, and ε_N is the nominal strain along the loading direction (i.e. the Z direction). The mean normalized displacement of particles is given by

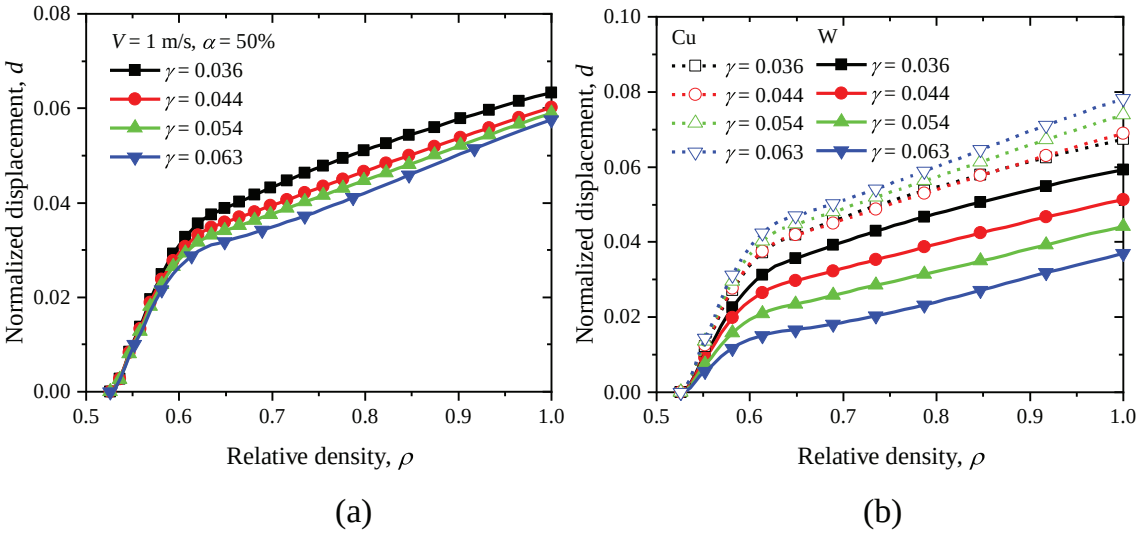

Fig. 11. (a) The mean normalized displacements of Cu—W composite powders with different inhomogeneity indexes and (b) the mean normalized displacements of Cu particles and W particles.

$$d = \frac{1}{N}\sum_{i=1}^{N} d_i \tag{9}$$

The mean normalized displacements of Cu—W composite powders with different inhomogeneity indexes and those of Cu particles and W particles separately are shown in Fig. 11. Similar to the evolution trend of rotation degree, the more uniform the composite powders are, the larger the mean normalized displacement is. As can be seen in Fig. 11(b), the change of the mean normalized displacement of W particles is greater than that of Cu particles. In addition, the difference in the mean normalized displacement between Cu and W particles decreases with the decrease of the inhomogeneity index. It is because in the relatively uniform composite powders, the stable packing structures formed by the contacted W particles are relatively few, and the Cu and W particles move almost consistently. Therefore, both the particle rotation and the particle translation can reflect the contribution of particle rearrangement to densification.

3.1.3. Meso-structural analysis and characterization

The deformation and stress evolution of local structure during compaction can be clearly observed in the MPFEM simulation. Several typical clusters (structures A, B, C, and D in Fig. 12), which are frequently appeared when the volume ratio of W and Cu is close to 1:1, are analyzed to reveal the meso-scale densification mechanism. The four clusters are selected by analyzing the contact relationship of all particles and it is found that their locations are random. Fig. 13 gives the von Mises stress distribution and the meso-scale deformation of these structures under different pressures.

Structure A consists of Cu particles only. These particles are obviously deformed with the increase of compaction pressure. The contact mode of two adjacent particles changes gradually from point contact to face contact, which indicates that the deformation is uniform when Cu particles gather together.

Different from structure A, structure B consists of W particles only. Due to the high strength of W, the plastic deformation of W particles is small, and the densification process of structure B is hard, so the large pore remains. To make structure B denser, a much higher compression pressure is required. The stress near the edge where particles come into contact with each other is greater than that in the interior of the particle, and high stress is maintained throughout the whole compaction process.

When a W particle is surrounded by a group of Cu particles (structure C), large plastic deformation occurs in the Cu particles but only slight deformation appears in the W particle. This meso-structure facilitates densification since less stress is required to achieve a higher relative density.

In the case of structure D, i.e. a Cu particle is surrounded by a cluster of W particles, the inner Cu particle deforms and fills the adjacent pore efficiently while the W particles experience small deformation. Compared to structure B, this meso-structure is relatively easier to fill pores under compression.

The deformation patterns and von Mises stress distribution of the central particle in structures A, B, C and D under pressures of 2, 50, 100 and 400 MPa are shown in Fig. 14. Similar to the equivalent strain of a particle, the equivalent von Mises stress of a particle can be defined by [5].

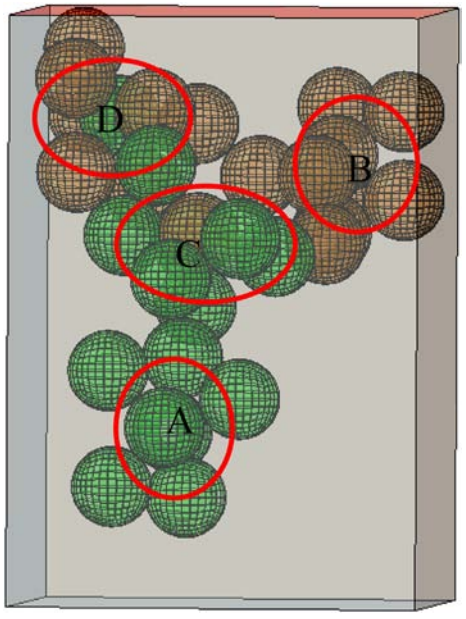

Fig. 12. Location of clusters A-D.

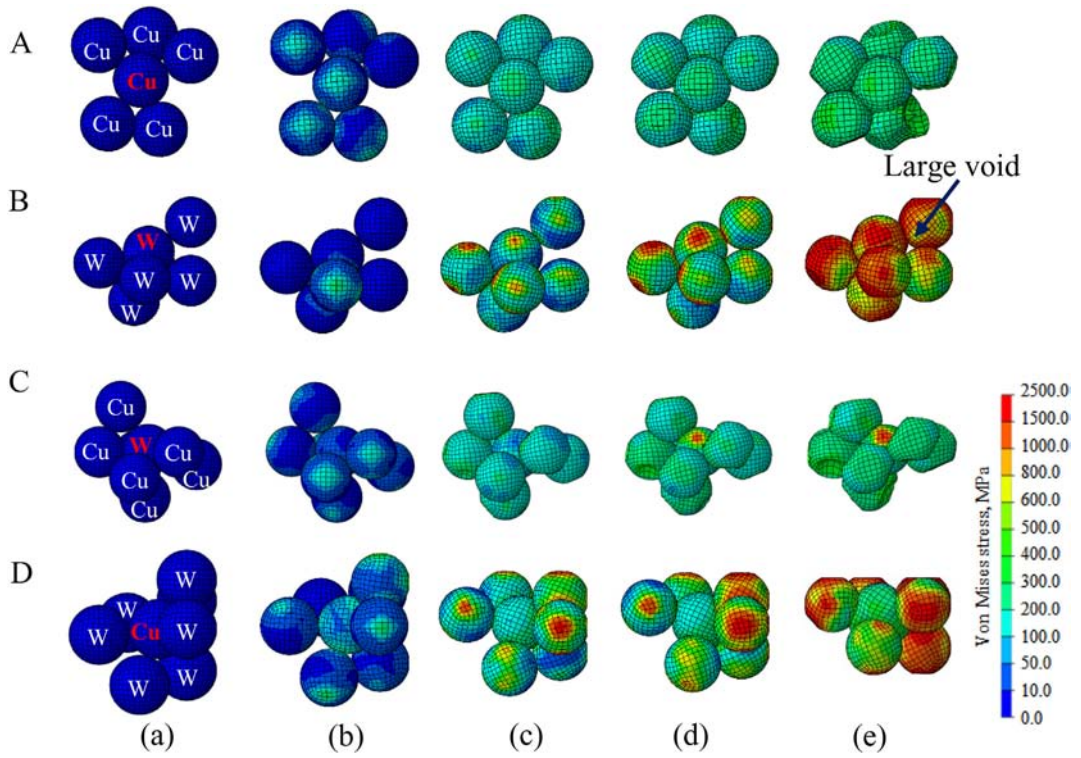

Fig. 13. The von Mises stress distribution and the meso-deformation of structures A, B, C and D under different pressures: (a) $p = 0$ MPa, (b) $p = 2$ MPa, (c) $p = 50$ MPa, (d) $p = 100$ MPa and (e) $p = 400$ MPa.

$$\sigma_{eq} = \sum_{j=1}^{N_E} \sigma^j{}_{von}/N_E \tag{10}$$

where N_E is the element number of a particle and equals 2048 in this study, and $\sigma^j{}_{von}$ is the von Mises stress of the j-th element in the particle. From Fig. 14(b), it is worthy to note that the particle in the center of structure B is almost unstressed until the relative density reaches a certain level. The reason is that the surrounding W particles form an arch structure like a shield and bear external loads, thus limiting the deformation of the W particle. With the increase of compaction pressure, the arch structure disappears and turns to an extrusion structure, where the stress of the central particle rises quickly as the extrusion from the adjacent W particles. The extrusion structure formed by contacted W particles is not conducive to powder compaction, resulting in uneven pores and stress concentration. However, in some cases, the arch structure and extrusion structure may be helpful to the powder compaction, such as structures C and D. From Figs. 14(a) and (b), it is found that the equivalent von Mises stress of the W particle in structure C is much smaller than that of W particle in structure B, as the arch structure formed by adjacent Cu particles in structure C 'protecting' the central W particle. Besides, the Cu particle in structure D deforms more severely than the Cu particle in structure A. As expected, the equivalent strain of the central W particle in structure C is smaller than that in structure B, and the equivalent strain of the central Cu particle in structure D is greater than that in structure A, as shown in Fig. 13(c).

Based on the above analysis, it could be concluded that structure B impedes powder densification severely and leads to a large residual void. The statistics of structure B in the samples with different inhomogeneity indexes are shown in Fig. 15, it is found that the number of structure B in these samples increases with the increase of inhomogeneity index. Therefore, the compaction pressure required to reach the same relative density is higher for non-uniform composite powders, especially in the particle deformation stage.

3.2. Effect of the initial relative density of composite powders

The effect of the initial relative density of powders on the densification process was explored by the configurations illustrated in Figs. 2(a)-(e), where the initial relative densities are 0.476, 0.510, 0.526, 0.537 and 0.558, respectively. The results in Fig. 16 indicate that the initial relative density has an obvious influence on powder compaction. The compaction pressure required to achieve the same relative density decreases with the increase of the initial relative density. The densification process is greatly affected by the initial relative density of powders in Stages 1 and 2. The reason probably is that the densification in Stages 1 and 2 is relevant to initial porosity, which depends on the initial relative density. And then with the increase of compaction pressure, the deformation mode turns from particle rearrangement to plastic deformation, which is independent of the porosity, and thus the p–ρ curves converge in Stage 3.

The fitting results of compaction data with Heckel equation are shown in Fig. 17(a), and the values of λ and β corresponding to different initial relative densities are plotted in Fig. 17(b). As can be seen, the value of λ decreases with the increase of the initial relative density, which shows that the powder with high initial relative density is tough to be densified by plastic deformation. Differently, the value of β increases with the increase of the initial relative density, indicating that the inter-particle motion is impeded in the initial dense powder.

The deformation mechanism of composite powder with different initial relative densities can also be quantitatively analyzed. As can be seen from Fig. 18(a), in the initial compression stage, the mean equivalent strains of Cu—W composite powders with different initial relative densities are almost zero, while in the subsequent compression stages, the mean equivalent strain of the composite powders with a lower initial relative density is larger than that with a higher one. Similarly, for the Cu—W composite powders with different initial relative densities, in the initial compression stage, the mean rotation degree increases quickly but in the subsequent compression stages, it increases slowly.

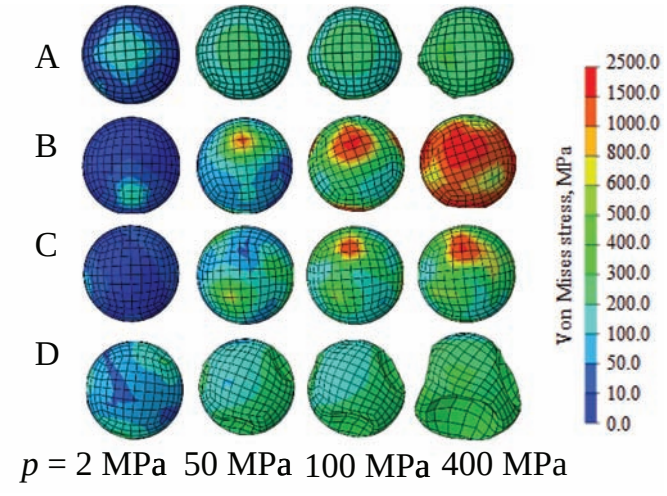

Fig. 14. The deformation of the central particle in structures A, B, C and D under pressures of 2, 50, 100 and 400 MPa (a); the equivalent von Mises stress (b) and the equivalent strain (c) of the central particle in structures A, B, C and D under compaction.

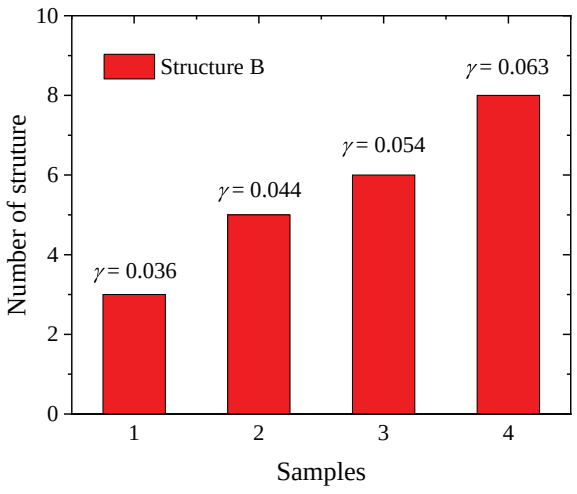

Fig. 15. The statistics of structure B in the samples with different inhomogeneity indexes.

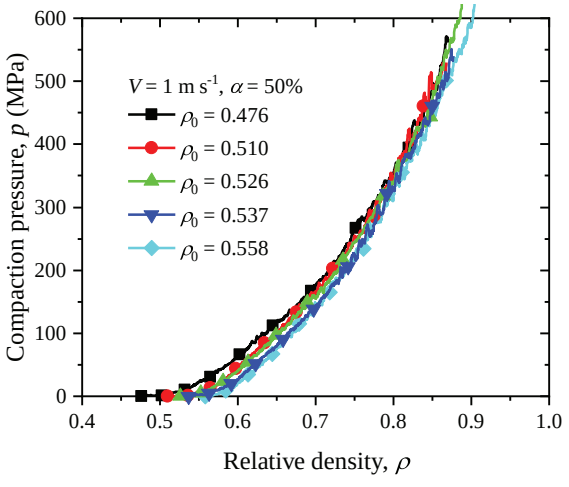

Fig. 16. Compaction pressure vs. relative density curves of Cu—W composite powders with different initial relative densities.

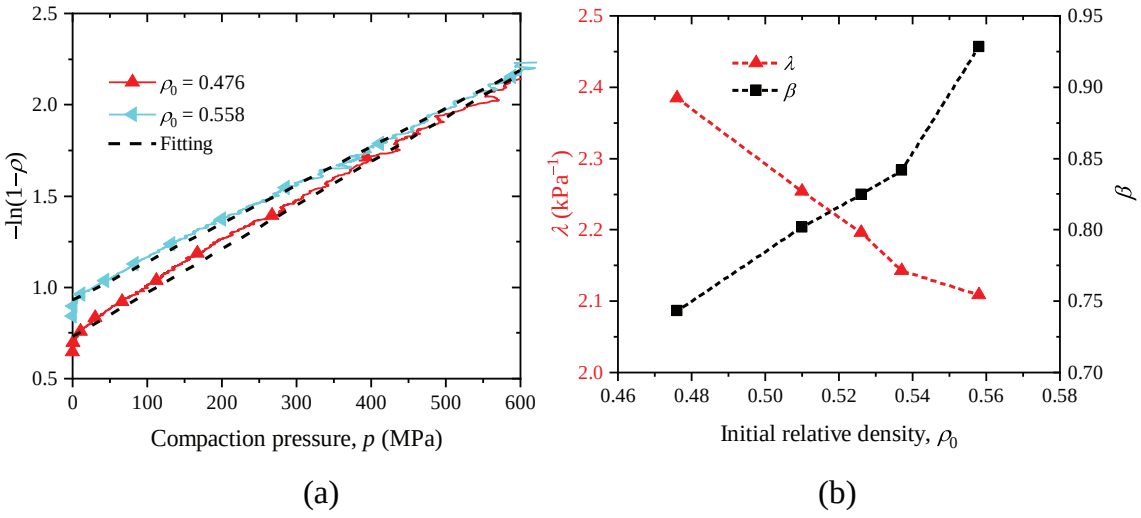

Fig. 17. (a) Fitting the MPFEM data with Heckel equation and (b) the parameters λ and β in the Heckel equation for different initial relative densities.

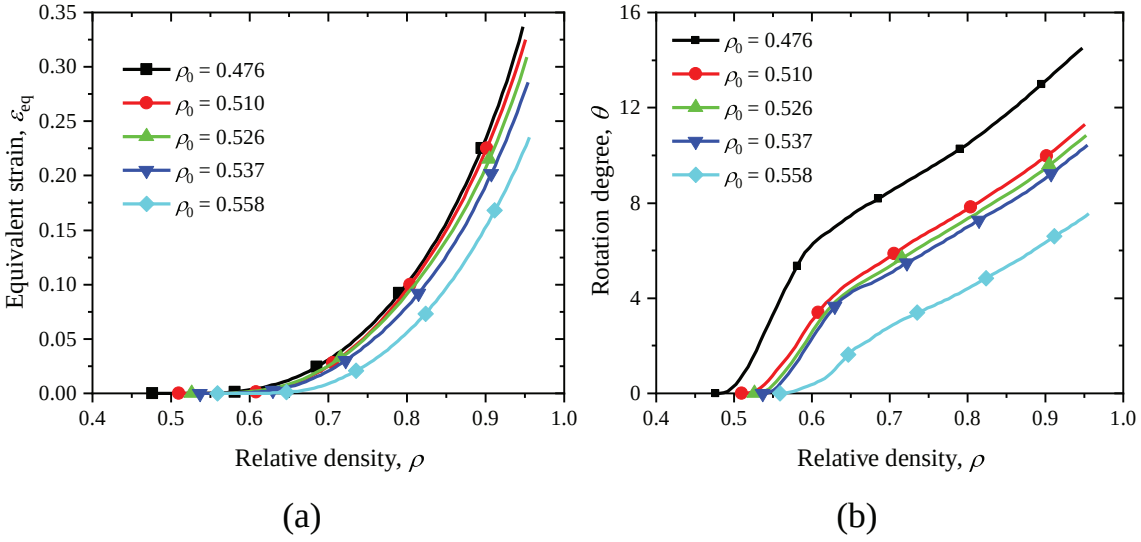

Fig. 18. The mean equivalent strains (a) and the mean rotation degrees (b) of Cu—W composite powders with different initial relative densities.

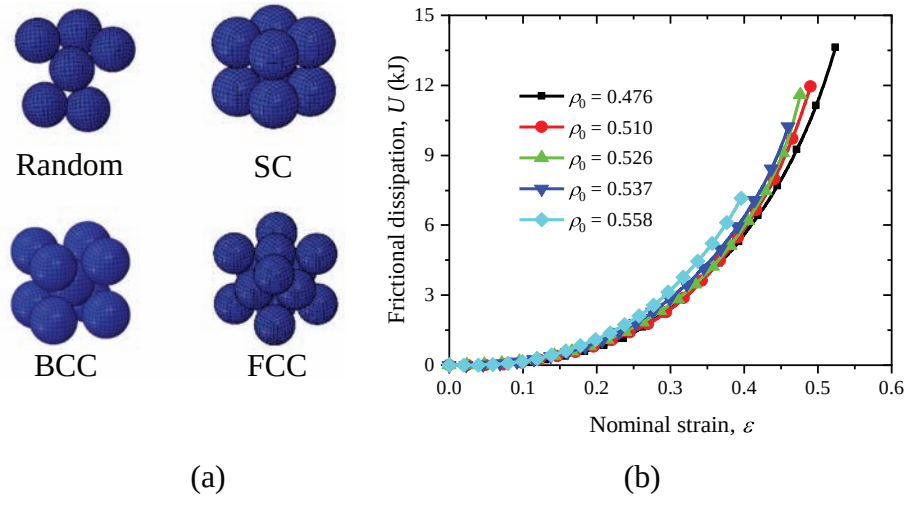

Fig. 19. (a) Different local packing modes (b) and the frictional dissipation of Cu—W composite powders with different initial relative densities during the compression process.

It is interesting to note that although the mean rotation degree of the composite powders with a higher initial relative density is smaller, the growth rates of all samples in Stages 2 and 3 are almost the same, as shown in Fig. 18(b). The results show that both the particle rearrangement and deformation are sensitive to the initial packing density of composite powders.

The smaller voids formed in the samples with high initial packing density are much easier to be filled by the deformation of adjacent particles during compaction. Thus, for a given pressure, the relative densities of these samples are much large. Local packing modes in powder normally include random packing, simple cubic (SC) packing, body centered cubic (BCC) and face centered cubic (FCC) packing [5,32], among which the porosity of BCC and FCC structures are relatively small, as illustrated in Fig. 19(a). The number of BCC and FCC structures in the initial dense powder is much larger than that in the initial loose powders and thus the average contact number of the initial dense powder is larger than that of the initial loose powder. The increase of the particle contact will increase the energy dissipation due to more inter-particle friction when the external loading is identical. Therefore, the frictional dissipation of initial dense powders is larger than that of initial loose powders when the nominal strain under uniaxial compression is the same, but the total frictional dissipation of initial dense powders is less than that of initial loose ones, as seen in Fig. 19(b). This phenomenon was also observed for composite powders with different size ratios [36]. Therefore, a higher initial packing density is not only beneficial to material transportation and storage, but also important to improve the preparation efficiency of intermetallic granular materials.

4. Conclusions

The mechanical behaviors of Cu—W composite powders under quasi-static compaction were investigated macroscopically and microscopically by using the multi-particle finite element method. Parametric studies including the initial relative density and the particle distribution of Cu—W composite powders on the process of powder compaction were conducted. The deformation, stress transmission and distribution, local relative density and distribution, and pores filling process and mechanism were analyzed from the particle level.

Pores can be filled by rearrangement of particles and plastic deformation of Cu particles. Particle rotation and deformation were quantitatively characterized by introducing a rotation degree and an equivalent strain of a particle. Based on the quantitative analysis of particle rearrangement and deformation, the process of pores filling mainly consists of three stages. In Stage 1, it is achieved by simply translating particles, and the deformation of particles is very small. In Stage 2, pores are filled through large plastic deformation of Cu particles, making the composite powder much denser. In Stage 3, the higher pressure causes further plastic deformation of W and Cu particles but in this stage, the increase of relative density is not significant due to the high yield stress of W particles and the constraints from neighboring particles.

The effect of the initial relative density on the mechanical response of Cu—W composite powders under compression is significant. Under the same compaction pressure, the relative density increases with the increase of the initial relative density at Stages 1 and 2. In addition, the Cu—W distribution of composite powders has a significant effect on the particle deformation stage. The more uniform the powder is, the easier it is to compress. However, at the initial compression stage, the particle rearrangement is insensitive to the particle distribution.

The meso-structure of composite powder plays an important role in the macroscopic mechanical behavior of its compaction. A meso-structure that consists of only W particles seriously hinders the densification process and makes the distribution of pores uneven. During compression, the stress is mainly concentrated in this structure, and then strong force chains are formed to hinder the compression. The resistance decreases with the increase of powder uniformity.

The present study indicates that the product quality may be improved by improving the powder uniformity or increasing the initial packing density. In addition, although the specific mixture of Cu and W particles is taken as the research object, the densification mechanisms are also applicable to the composite powders with the combination of hard and soft particles.

In addition to powder compaction, solid-state sintering of composite powders is also significantly important. Future work may be focused on the effects of sintering temperature and heating rate on the densification processes and mechanisms of Cu—W composite powders for optimizing the adjustable parameters in the sintering stage to form superior products. And, systematic researches about the whole powder metallurgy process based on numerical simulation are meaningful. It can be used to guide the production for improving the mechanical proprieties of the final products by process optimization.

Declaration of Competing Interest

The authors declare that they have no known competing financial interests or personal relationships that could have appeared to influence the work reported in this paper.

Acknowledgement

This work is supported by the Fundamental Research Funds for the Central Universities (Grant No. WK2480000003).

References

[1] K. Morsi, V.V. Patel, Processing and properties of titanium-titanium boride (TiB_w) matrix composites–a review, J. Mater. Sci. 42 (2007) 2037–2047, https://doi.org/10.1007/s10853-006-0776-2.
[2] S.M. Choi, H. Awaji, Nanocomposites–a new material design concept, Sci. Technol. Adv. Mater. 6 (2005) 2–10, https://doi.org/10.1016/j.stam.2004.06.002.
[3] V. Viswanathan, T. Laha, K. Balani, A. Agarwal, S. Seal, Challenges and advances in nanocomposite processing techniques, Mater. Sci. Eng. R 54 (2006) 121–285, https://doi.org/10.1016/j.mser.2006.11.002.
[4] L.M. Zhang, W.S. Chen, G.Q. Luo, P.G. Chen, Q. Shen, C.B. Wang, Low-temperature densification and excellent thermal properties of W-Cu thermal-management composites prepared from copper-coated tungsten powders, J. Alloys Compd. 588 (2014) 49–52, https://doi.org/10.1016/j.jallcom.2013.11.003.
[5] Y. Zou, X.Z. An, Q. Jia, R.P. Zou, A.B. Yu, Three-dimensional MPFEM modelling on isostatic pressing and solid phase sintering of tungsten powders, Powder Technol. 354 (2019) 854–866, https://doi.org/10.1016/j.powtec.2019.07.013.
[6] P. Zhao, S.B. Guo, G.H. Liu, Y.X. Chen, J.T. Li, Fabrication of Cu-riched W–Cu composites by combustion synthesis and melt-infiltration in ultrahigh-gravity field, J. Nucl. Mater. 441 (2013) 343–347, https://doi.org/10.1016/j.jnucmat.2013.06.011.
[7] J. Fan, T. Liu, S. Zhu, Y. Han, Synthesis of ultrafine/nanocrystalline W–(30–50)Cu composite powders and microstructure characteristics of the sintered alloys, Int. J. Refract. Met. Hard Mater. 30 (2012) 33–37, https://doi.org/10.1016/j.ijrmhm.2011.06.011.
[8] A. Abu-Oqail, M. Ghanim, M. El-Sheikh, A. El-Nikhaily, Effects of processing parameters of tungsten-copper composites, Int. J. Refract. Met. Hard Mater. 35 (2012) 207–212, https://doi.org/10.1016/j.ijrmhm.2012.02.015.
[9] N.C. Kothari, Sintering kinetics in tungsten powder, J. Less Common Met. 5 (1963) 140–150, https://doi.org/10.1016/0022-5088(63)90007-9.
[10] E. Olsson, P.-L. Larsson, A numerical analysis of cold powder compaction based on micromechanical experiments, Powder Technol. 243 (2013) 71–78, https://doi.org/10.1016/j.powtec.2013.03.040.
[11] S.H. Chung, H. Park, K.D. Jeon, K.T. Kim, S.M. Hwang, An optimal container design for metal powder under hot isostatic pressing, J. Eng. Mater. Technol. 123 (2001) 234–239, https://doi.org/10.1115/1.1354992.
[12] E. Armentani, G.F. Bocchini, G. Cricrì, R. Esposito, Metal powder compacting dies: optimised design by analytical or numerical methods, Powder Metall. 46 (2003) 349–360, https://doi.org/10.1179/003258903225008607.
[13] A.R. Khoei, A.R. Sameti, H. Mofatteh, Compaction simulation of crystalline nanopowders under cold compaction process with molecular dynamics analysis, Powder Technol. 373 (2020) 741–753, https://doi.org/10.1016/j.powtec.2020.06.069.
[14] N.A. Fleck, On the cold compaction of powders, J. Mech. Phys. Solids 43 (1995) 1409–1431, https://doi.org/10.1016/0022-5096(95)00039-l.
[15] K. Biswas, Comparison of various plasticity models for metal powder compaction processes, J. Mater. Process. Technol. 166 (2005) 107–115, https://doi.org/10.1016/j.jmatprotec.2004.08.006.
[16] S.M. Tahir, A.K. Ariffin, M.S. Anuar, Finite element modelling of crack propagation in metal powder compaction using Mohr–Coulomb and Elliptical Cap yield criteria,

Powder Technol. 202 (2010) 162–170, https://doi.org/10.1016/j.powtec.2010.04.033.
[17] P.A. Cundall, O.D.L. Strack, A discrete numerical model for granular assemblies, Geotechnique 29 (1979) 47–65, https://doi.org/10.1680/geot.1979.29.1.47.
[18] H. Jonsson, G. Alderborn, G. Frenning, Evaluation of bulk compression using a discrete element procedure calibrated with data from triaxial compression experiments on single particles, Powder Technol. 345 (2019) 74–81, https://doi.org/10.1016/j.powtec.2018.12.090.
[19] D.M. Wang, Y.H. Zhou, Particle dynamics in dense shear granular flow, Acta Mech. Sinica 26 (2010) 91–100, https://doi.org/10.1007/s10409-009-0322-y.
[20] X.Z. An, R.Y. Yang, K.J. Dong, R.P. Zou, A.B. Yu, Micromechanical simulation and analysis of one-dimensional vibratory sphere packing, Phys. Rev. Lett. 95 (2005) 205502, https://doi.org/10.1103/physrevlett.95.205502.
[21] E. Olsson, P.-L. Larsson, Micromechanical investigation of the fracture behavior of powder materials, Powder Technol. 286 (2015) 288–302, https://doi.org/10.1016/j.powtec.2015.08.018.
[22] C.L. Martin, D. Bouvard, Isostatic compaction of bimodal powder mixtures and composites, Int. J. Mech. Sci. 46 (2004) 907–927, https://doi.org/10.1016/j.ijmecsci.2004.05.012.
[23] D.T. Gethin, R.S. Ransing, R.W. Lewis, M. Dutko, A.J.L. Crook, Numerical comparison of a deformable discrete element model and an equivalent continuum analysis for the compaction of ductile porous material, Comput. Struct. 79 (2001) 1287–1294, https://doi.org/10.1016/s0045-7949(01)00015-3.
[24] A. Zavaliangos, A numerical study of the development of tensile principal stresses during die compaction, Part. Sci. Technol. 21 (2003) 105–115, https://doi.org/10.1080/02726350307489.
[25] A.T. Procopio, A. Zavaliangos, Simulation of multi-axial compaction of granular media from loose to high relative densities, J. Mech. Phys. Solids 53 (2005) 1523–1551, https://doi.org/10.1016/j.jmps.2005.02.007.
[26] G. Frenning, An efficient finite/discrete element procedure for simulating compression of 3D particle assemblies, Comput. Methods Appl. Mech. Eng. 197 (2008) 4266–4272, https://doi.org/10.1016/j.cma.2008.05.002.
[27] G. Frenning, Compression mechanics of granule beds: a combined finite/discrete element study, Chem. Eng. Sci. 65 (2010) 2464–2471, https://doi.org/10.1016/j.ces.2009.12.029.
[28] B. Harthong, D. Imbault, P. Dorémus, The study of relations between loading history and yield surfaces in powder materials using discrete finite element simulations, J. Mech. Phys. Solids 60 (4) (2012) 784–801, https://doi.org/10.1016/j.jmps.2011.11.009.
[29] S.W. Yan, S.Y. Huang, W. Liu, J.H. Hu, Y. Lei, M.C. Zhou, Experimental and numerical investigation of temperature evolution during electromagnetic pulsed compaction of powders, Powder Technol. 306 (2017) 1–9, https://doi.org/10.1016/j.powtec.2016.11.014.
[30] J. Zhang, A study of compaction of composite particles by multi-particle finite element method, Compos. Sci. Technol. 69 (2009) 2048–2053, https://doi.org/10.1016/j.compscitech.2008.11.020.
[31] F. Huang, X.Z. An, Y.X. Zhang, A.B. Yu, Multi-particle FEM simulation of 2D compaction on binary Al/SiC composite powders, Powder Technol. 314 (2017) 39–48, https://doi.org/10.1016/j.powtec.2017.03.017.
[32] Y.X. Zhang, X.Z. An, Y.L. Zhang, Multi-particle FEM modeling on microscopic behavior of 2D particle compaction, Appl. Phys. A Mater. Sci. Process. 118 (2015) 1015–1021, https://doi.org/10.1007/s00339-014-8861-x.
[33] X.J. Xin, P. Jayaraman, G. Jiang, R.H. Wagoner, G.S. Daehn, Explicit finite element method simulation of consolidation of monolithic and composite powders, Metall. Mater. Trans. A 33 (2002) 2649–2658, https://doi.org/10.1007/s11661-002-0386-9.
[34] J. Zhou, C.Y. Zhu, W. Zhang, W.T. Ai, X.J. Zhang, K. Liu, Experimental and 3D MPFEM simulation study on the green density of Ti–6Al–4V powder compact during uniaxial high velocity compaction, J. Alloys Compd. 817 (2020) 153226, https://doi.org/10.1016/j.jallcom.2019.153226.
[35] P. Han, X.Z. An, Y.X. Zhang, F. Huang, T.X. Yang, H.T. Fu, X.H. Yang, Z.S. Zou, Particulate scale MPFEM modeling on compaction of Fe and Al composite powders, Powder Technol. 314 (2016) 69–77, https://doi.org/10.1016/j.powtec.2016.11.021.
[36] P. Han, X.Z. An, D.F. Wang, H.T. Fu, X.H. Yang, H. Zhang, Z.S. Zou, MPFEM simulation of compaction densification behavior of Fe-Al composite powders with different size ratios, J. Alloys Compd. 741 (2018) 473–481, https://doi.org/10.1016/j.jallcom.2018.01.198.
[37] B. Zhao, X.Z. An, H.Y. Zhao, D.Z. Gou, L.L. Shen, X.D. Sun, DEM simulation on random packings of binary tetrahedron-sphere mixtures, Powder Technol. 361 (2020) 160–170, https://doi.org/10.1016/j.powtec.2019.09.055.
[38] H. Asgharzadeh, A. Simchi, H.S. Kim, A plastic-yield compaction model for nanostructured Al6063 alloy and Al6063/Al2O3 nanocomposite powder, Powder Technol. 211 (2011) 215–220, https://doi.org/10.1016/j.powtec.2011.04.020.
[39] Z.R. Hesabi, H.R. Hafizpour, A. Simchi, An investigation on the compressibility of aluminum/nano-alumina composite powder prepared by blending and mechanical milling, Mater. Sci. Eng. A 454 (2007) 89–98, https://doi.org/10.1016/j.msea.2006.11.129.
[40] T.J. Vogler, M.Y. Lee, D.E. Grady, Static and dynamic compaction of ceramic powders, Int. J. Solids Struct. 44 (2007) 636–658, https://doi.org/10.1016/j.ijsolstr.2006.05.001.
[41] M.A. Meyers, D.J. Benson, E.A. Olevsky, Shock consolidation: microstructurally-based analysis and computational modeling, Acta Mater. (7) (1999) 2089–2108, https://doi.org/10.1016/s1359-6454(99)00083-x.
[42] Z.Z. Xie, X.Z. An, X.H. Yang, C.X. Li, Y.S. Shen, Numerical realization and structure characterization on random close packings of cuboid particles with different aspect ratios, Powder Technol. 344 (2019) 514–524, https://doi.org/10.1016/j.powtec.2018.12.017.
[43] X. Chen, W. Sun, X.J. Li, X.H. Wang, H.H. Yan, K.B. Li, Experimental and numerical studies on W–Cu functionally graded materials produced by explosive compaction–welding sintering, Fusion Eng. Des. 137 (2018) 349–357, https://doi.org/10.1016/j.fusengdes.2018.10.016.
[44] M. Richou, F. Gallay, B. Böswirth, I. Chu, G. Dose, H. Greuner, G. Kermouche, M. Lenci, T. Loewenhoff, R. Maestracci, E. Meillot, M. Missirlian, J.Y. Pastor, A. Quet, S. Roccella, E. Tejado, M. Wirtz, E. Visca, G. Pintsuk, J.H. You, Performance assessment of thick W/Cu graded interlayer for DEMO divertor target, Fusion Eng. Des. 157 (2020) 111610, https://doi.org/10.1016/j.fusengdes.2020.111610.
[45] A. Yusefi, N. Parvin, Fabrication of three layered W-Cu functionally graded composite via spark plasma sintering, Fusion Eng. Des. 114 (2017) 196–202, https://doi.org/10.1016/j.fusengdes.2016.11.013.
[46] G.R. Johnson, W.H. Cook, Fracture characteristics of three metals subjected to various strains, strain rates, temperatures and pressures, Eng. Fract. Mech. 21 (1985) 31–48.
[47] K.D. Dai, P.W. Chen, Numerical simulation of the shock compaction of W/Cu powders, Mater. Sci. Forum 673 (2011) 113–118, https://doi.org/10.4028/www.scientific.net/MSF.673.113.
[48] B. Zhang, X.B. Li, D. Li, Assessment of thermal expansion coefficient for pure metals, Calphad 43 (2013) 7–17, https://doi.org/10.1016/j.calphad.2013.08.006.
[49] K.T. Kim, J.H. Cho, J.S. Kim, Cold compaction of composite powders, J. Eng. Mater. Technol. 122 (2000) 119–128, https://doi.org/10.1115/1.482775.
[50] R.W. Heckel, Density-pressure relationship in powder compaction, Trans. Metall. Soc. AIME 221 (1961) 671–675.
[51] J.C. Hart, G.K. Francis, L.H. Kauffman, Visualizing quaternion rotation, ACM T. Graph. 13 (1994) 256–276, https://doi.org/10.1145/195784.197480.